OPEN ACCESS Freely available online

PLOS ONE

Improper Tagging of the Non-Essential Small Capsid Protein VP26 Impairs Nuclear Capsid Egress of Herpes Simplex Virus

Claus-Henning Nagel[1☯¤], Katinka Döhner[1☯], Anne Binz[1], Rudolf Bauerfeind[2], Beate Sodeik[1]*

1 Institute of Virology, Hanover Medical School, Hanover, Germany, **2** Institute of Cell Biology, Hanover Medical School, Hanover, Germany

Abstract

To analyze the subcellular trafficking of herpesvirus capsids, the small capsid protein has been labeled with different fluorescent proteins. Here, we analyzed the infectivity of several HSV1(17$^+$) strains in which the N-terminal region of the non-essential small capsid protein VP26 had been tagged at different positions. While some variants replicated with similar kinetics as their parental wild type strain, others were not infectious at all. Improper tagging resulted in the aggregation of VP26 in the nucleus, prevented efficient nuclear egress of viral capsids, and thus virion formation. Correlative fluorescence and electron microscopy showed that these aggregates had sequestered several other viral proteins, but often did not contain viral capsids. The propensity for aggregate formation was influenced by the type of the fluorescent protein domain, the position of the inserted tag, the cell type, and the progression of infection. Among the tags that we have tested, mRFPVP26 had the lowest tendency to induce nuclear aggregates, and showed the least reduction in replication when compared to wild type. Our data suggest that *bona fide* monomeric fluorescent protein tags have less impact on proper assembly of HSV1 capsids and nuclear capsid egress than tags that tend to dimerize. Small chemical compounds capable of inducing aggregate formation of VP26 may lead to new antiviral drugs against HSV infections.

Citation: Nagel C-H, Döhner K, Binz A, Bauerfeind R, Sodeik B (2012) Improper Tagging of the Non-Essential Small Capsid Protein VP26 Impairs Nuclear Capsid Egress of Herpes Simplex Virus. PLoS ONE 7(8): e44177. doi:10.1371/journal.pone.0044177

Editor: Bruce W. Banfield, Queen's University, Canada

Received June 4, 2012; **Accepted** July 30, 2012; **Published** August 31, 2012

Funding: This study was supported by the German Research Council (DFG-SPP1175 to BS and RB; DFG-SFP900 to BS), and the European Union 6th Framework Program (EU-NEST AXON SUPPORT, contract number 12702 to BS). The funders had no role in study design, data collection and analysis, decision to publish, or preparation of the manuscript.

Competing Interests: The authors have declared that no competing interests exist.

* E-mail: sodeik.beate@mh-hannover.de

☯ These authors contributed equally to this work.

¤ Current address: Heinrich-Pette-Institute – Leibniz Institute for Experimental Virology, Hamburg, Germany

Introduction

Single and dual-color fluorescently tagged strains are valuable tools to elucidate the intracellular trafficking of virions and subviral particles. In an ideal case, the modified strain replicates with the same kinetics and to the same titers as its parental strain, and the tag neither interferes with any step of the viral life cycle, nor changes the biochemical properties of the modified viral structure. For herpesviruses, fluorescent protein (FP) domains attached to the small capsid protein (SCP) have been used extensively to characterize the molecular mechanisms of virus assembly and egress or nuclear targeting of incoming capsids in cells and biochemical assays (c.f. Fig.1; [1–13]). The SCPs are recruited to capsids via the major capsid proteins (MCP). Although similar building principles apply, the amino acid sequences of both, SCPs and MCPs vary considerably among the herpesviruses [14–18]. SCPs are essential for the replication of human and mouse cytomegalovirus, Epstein-Barr virus and Kaposis sarcoma-associated herpesvirus, but not for the alphaherpesviruses herpes simplex virus type 1 (HSV1), pseudorabiesvirus (PrV) or varizella zoster virus (VZV; [7,8,19–23]). However, HSV1 strains lacking the SCP yield lower titers than wild type in the murine eye and trigeminal ganglion after corneal infection as well as in BHK cells [8,20,24]. PrV lacking the SCP is also less neuroinvasive and grows to lower titers in cell culture, while the SCP of VZV is essential for infection of the human skin xenograft murine model and of melanoma cells but not of embryonic lung fibroblasts [7,25].

VP26, the SCP of HSV1, is a basic 12 kDa protein of 112 amino acid residues (aa) with low solubility and encoded by the gene UL35 [26,27]. In solution, it is only 13 to 15% α-helical but is 80% β-sheet, and a secondary-structure algorithm predicts two α-helical regions between aa 13 to 31 and 42 to 72 [26,28,29]. Herpesvirus capsids are assembled in the nucleus and for its nuclear import VP26 requires the interaction with VP5, the MCP of HSV1, and either capsid protein preVP22a or VP19c [30–32]. Hexamers of VP5 form the 150 hexons on the faces and edges, while pentamers of VP5 form the 11 pentons on the vertices of the icosahedral capsid. A virion can harbor up to 900 copies of VP26 as it decorates the top of the hexons in a hexamer [14,16,28]. The C-terminal half of HSV1-VP26, aa 50 to 112 are sufficient for binding to an interface of hydrophobic residues and small charged patches on the upper hexon domain [26,33]. Combined cryoelectron microscopy and *ab initio* modeling suggest a novel fold of the C-terminal aa 42 to 112 with three short α-helices [29,34]. While the hexons recruit VP26, the pentons serve as attachment sites for

A

HSV1 strains + constructs	Genomic Organization	FP	Plaque	Nuclear Aggregates	References
wild type	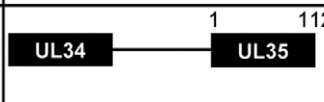		+++	–	Duff & Rapp 1973 Tanaka et al. 2003 Nagel et al. 2008
KOS-LacZ-VP26$_{\Delta aa10-102}$	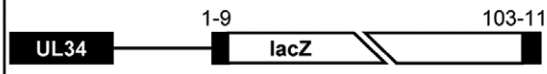		+++		Desai et al. 1998
(17+)blueLox-VP26$_{\Delta aa6-112}$	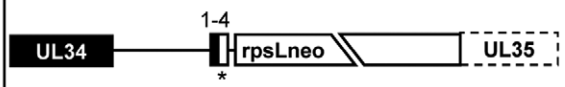		+++		Nagel et al. 2008
KOS-GFPVP26$_{\Delta aa1-7}$		dimer	++	++	Desai & Person 1998
(F)-GFPVP26$_{\Delta aa1-7}$		dimer	++	n.d.	Snyder et al. 2006
(17+)blueLox-mRFPVP26$_{\Delta aa1-7}$	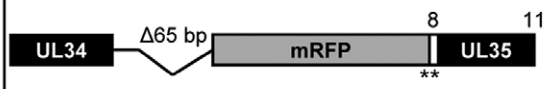	monomer	+++	–	Nagel et al. 2008
(17+)blueLox-GFPVP26$_{\Delta aa1-7}$ (-gDmRFP)		dimer	++	++	Nagel et al. 2008
(F)YEbac102-mRFPVP26$_{\Delta aa1-4}$	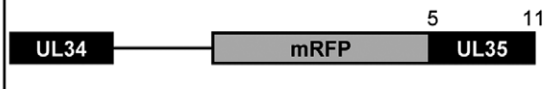	monomer	++	+	de Oliveira et al. 2008
(F)YEbac102-YFP^{Venus}VP26$_{\Delta aa1}$		monomer	++	+	Sugimoto et al. 2008
(F)YEbac102-mRFPVP26$_{\Delta aa1}$	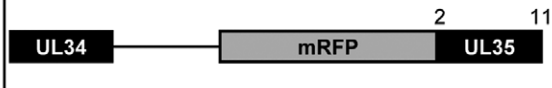	monomer	++	n.d.	Antinone et al. 2010
(17+)blueLox-GFPVP26$_{\Delta aa5-7}$		dimer	–	++	this study
(17+)blueLox-YFPVP26$_{\Delta aa5-7}$	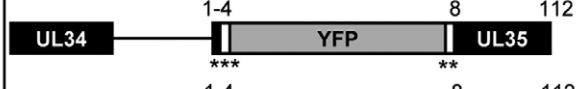	dimer	– –	+++	this study
(17+)blueLox-CFPVP26$_{\Delta aa5-7}$	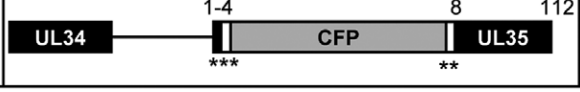	monomer	++	+	this study

B

```
ggc gcg cgc cta taa aaa agg acg cac cgc cgc cct aat cgc cag tgc gtt ccg gac gcc  wt
 G   A   R   L   -
ggc gcg cgc cta taa aaa agg acg cac cgc cgc cct aat cgc cag tgc gtt ccg gac gcc  Δaa5-7
 G   A   R   L   -
ggc gcg cgc cta taa aaa agg acg cac cgc cgc cct aat cgc cag tgc gtt ccg gac gcc  Δaa1-7
 G   A   R   L   -

ttc gcc cca cac agc cct ccc gac cga cac ccc cat atc gct tcc cga cct ccg gtc ccg  wt

ttc gcc cca cac agc cct ccc gac cga cac ccc cat atc gct tcc cga cct ccg gtc ccg  Δaa5-7

ttc gcc cca c-- --- --- --- --- --- --- --- --- --- --- --- --- --- --- --- ---  Δaa1-7

atg gcc gtc ccg caa ttt cac --- --- --- --- ... --- --- --- --- --- --- cgc ccc  wt
 M   A   V   P   Q   F   H                                                R   P
atg gcc gtc ccg caC TCG ACC ATG GTG AGC AAG ... GAG CTG TAC AAC TCG AGC cgc ccc  Δaa5-7
 M   A   V   P   H   S   T   M   V   S   K  ...  E   L   Y   N   S   S   R   P
--- --- --- --- --- TCG ACC ATG GTG AGC AAG ... GAG CTG TAC AAC TCG AGC cgc ccc  Δaa1-7
                     M   V   S   K  ...  E   L   Y   N   S   S   R   P
```

Figure 1. HSV1-VP26 constructs. (A) 1st column: HSV1 constructs in which the SCP VP26 has been tagged with different fluorescent protein domains. 2nd column: Genomic organization of the UL35 region approximately drawn to scale. The gene UL35 coding for VP26 has been disrupted by replacing it with lacZ or an rpsLneo cassette out of frame. Some constructs lack a 65 bp region upstream of UL35 (D65 bp) including the first seven N-terminal codons of VP26 (Daa1–7), while others lack only four (Δaa1–4) or just one (Daa1) codon. For the present study, the fluorescent protein tag was inserted between VP26 residues 4 and 8 (Daa5–7). Due to the mutagenesis, some strains contain additional linkers (*, AW; **, NSS; ***, HST). 3rd column: Propensity of the fluorescent protein (FP) to dimerize [76–80]. 4th column: Ability of the construct to replicate and to form plaques (+++, similar to wild type; ++ attenuated, but robust growth; − strongly attenuated, tiny plaques; −−, single fluorescent cells, no plaques). 5th column: Propensity of the construct to induce nuclear aggregates (+++, large irregular shaped aggregates; ++, large aggregates early after infection or transfection; +, aggregates late in infection; − aggregates in less than 2% of cells even late in infection). 6th column: References. (B) Nucleotide (upper lines) and amino acid (lower lines) sequences of the UL34/UL35 (pUL34/VP26) intergenic region. The 3¢ end of the UL34 ORF until the 5¢ start of the UL35 ORF are shown for wild type HSV-1, the GFPVP26$_{Äaa\mathbf{5}–7}$ (Äaa5–7) and GFPVP26$_{Äaa\mathbf{1}–7}$ (Äaa1–7) mutants. Additional nucleotides inserted during mutagenesis are shown in bold capitals, and the GFP amino acids are shown in italics. Putative Inr late promoter elements are underlined with the element perfectly matching the consensus sequence being underlined and in italics. The original amino acids encoded by UL35 are shown in bold capitals, the inserted GFP residues in italic capitals and the additional linker residues in normal script capitals.
doi:10.1371/journal.pone.0044177.g001

the tegument protein pUL36, and it has been suggested that this may be due to similarities between aa 66 to 96 of VP26 and aa 1712 to 1751 of pUL36 [14,29,35,36].

In addition to VP5, HSV1-VP26 can also interact with the capsid proteins VP23 and pUL25 as well as the tegument proteins pUL11, pUL14, pUL16, pUL21, pUL37, VP16, pUL51, and pUS3 in yeast-two-hybrid assays [33,37]. Yet, the incorporation of pUL37 and VP16 into HSV1 virions does not depend on VP26 but on pUL36 [38]. Furthermore HSV1-VP26 can bind to the host proteins tetraspanin-7 and the dynein light chains Tctex-1 and RP3 [33,39,40]. However, incoming capsids of HSV1-ΔVP26 can still utilize the microtubule motor dynein for transport to the nucleus, and HSV1-ΔVP26 capsids with inner tegument proteins on their surface can recruit dynein, whereas nuclear capsids devoid of inner tegument, but exposing VP26 cannot [5,13,20,21,41]. Thus, VP26 is not essential for binding dynein to viral capsids, but it may somehow regulate the interaction of dynein light chains with other host factors or the function of dynein.

The N-terminal region of the VP26 of HSV1 or PrV has been successfully used to insert a FP while maintaining infectivity (c.f. Fig. 1A; [2,4,7,8,10,11,42,43]). Cryoelectron microscopy tomography studies indicate that there are few highly ordered contacts between VP26 and the surrounding tegument, and most reported interaction partners employ its C-terminal half [24,26,33,35,36]. However the mass of the SCPs is tripled with additions such as mRFP (monomeric red FP) or GFP (green FP), CFP (cyan FP) or YFP (yellow FP) that have molecular weights of 25 to 27 kDa, and such tags can attenuate the replication of HSV1 and PrV in culture, and its pathogenesis in murine infection models [7,8,42,44].

Since the HSV1(17$^+$) strains that we had constructed previously exhibited prominent nuclear aggregates of GFPVP26 and reduced titers in BHK cells [8,42], we analyzed here several other strains in order to identify a less invasive FP tag. While some insertions were well tolerated, unexpectedly other additions prevented the formation of infectious HSV1 in spite of HSV1-VP26 not being essential. The non-infectious constructs had a very high propensity to form large nuclear aggregates of VP26 and were impaired in nuclear capsid egress, most likely by sequestering other essential proteins into these aggregates. The strain with the least invasive mRFP tag on VP26 induced few nuclear aggregates, and fewer impediments of nuclear egress, secondary envelopment and virion formation. It therefore provides a better backbone to construct new dual-color HSV1(17$^+$) variants with other FPs on tegument or glycoproteins. On the other hand, tags that promote mild VP26 aggregate formation may be used to identify further functional interactions with other structural HSV1 proteins by screening for additional synthetic lethal or rescuing mutations [45,46]. Our data furthermore imply that if compounds could be identified that induce SCP aggregation and thus prevent virion formation; even non-essential viral proteins could provide targets for antiviral therapy.

Materials and Methods

Ethics Statement

For immunofluorescence labeling (see below) we applied human serum of healthy, HSV1-seronegative volunteers. This procedure was approved by the Institution Review Board (*Ethikkommision* of Hannover Medical School, approval number 893). Written informed consent of the blood donors, according to the Institution Review Boards, was obtained.

Cells, Viruses and Antibodies

BHK-21 (ATCC CCL-10) and Vero (ATCC CCL-81) cells were cultured in Minimum Essential Medium (MEM) with 10% and 7.5% fetal calf serum, respectively. Retinal pigment epithelial (RPE) cells (ATCC CRL-4000) were grown in D-MEM/HAM F-12 1:1 with 10% fetal calf serum. HSV1 was propagated in BHK cells and purified as described previously [5,47]. For this study, we used virions pelleted from the medium of infected cells. The strains HSV1(17$^+$) and HSV1(KOS)-GFPVP26$_{\Delta aa1–7}$ (HSV1-K26GFP) were kindly provided by John Subak-Sharpe (MRC Virology Unit, Glasgow, UK) and Prashant Desai (Johns Hopkins University, Baltimore, MD), respectively [42,48]. All virus stocks were titrated on Vero cells [49]. Rabbit polyclonal antibodies (PAb) directed against empty capsids (α-LC; [50]), VP26$_{aa95–112}$ [20], VP5 (α-NC-1; [50]), VP22a (α-NC-3,4; [50]), VP23 (α-NC-5; [50]), pUL25 (ID1, R8–3; [51,52]), pUL36$_{aa1408–2112}$ (#147; [13,41]), pUL36$_{aa3048–3057}$ (C-term; [53]), pUS3 [54], pUL34 [55], or human PML protein$_{aa157–394}$ (H-238; Santa Cruz Biotechnology Inc., Santa Cruz, CA), as well as the mouse monoclonal antibodies (MAb) against VP5 (5C10, 8F5; [56]; LP12; [57]; H1.4 [Biodesign International, Saco, ME]), VP23 (1D2; [58]), pUL25 and pUL17 (#166, #203; [59]), or ICP8 (HB8180, ATCC, Rockville, MD, USA; provided by Regine Heilbronn, Charité-UniversitΔtsmedizin, Berlin, Germany) were used.

Construction of HSV1 Strains with Tagged VP26

In our previously described strains HSV1(17$^+$)blueLox-mRFPVP26 and -GFPVP26, the fluorescent protein sequences had been inserted into the VP26 sequence by deleting a 65 bp sequence including the first seven VP26 codons for Met-Ala-Val-Pro-Glu-Phe-His (c.f. Fig. 1B; [8]; P. Desai, personal communication). Therefore, in the present study they are called HSV1(17$^+$)blueLox-mRFPVP26$_{\Delta aa\mathbf{1}–7}$ and -GFPVP26$_{\Delta aa\mathbf{1}–7}$. In HSV1(17$^+$)blueLox-GFPVP26$_{\Delta aa\mathbf{1}–7}$-gDmRFP, glycoprotein D has also been labeled with monomeric RFP at its C-terminus;

this virus has been named HSV1(17$^+$)blueLox-GFPVP26-gDmRFP previously [8]. To construct additional HSV1 strains in which aa 5 to 7 (Glu-Phe-His) of VP26 were replaced by the fluorescent protein sequence as originally proposed by Desai & Person (1998), first an *Xho*I site was inserted into the ORF UL35. To this end, 500 bp upstream of the insertion site were amplified with *NNN NNN CCT GCA GG*A TGC CCG GCC GAT GAT GG and *NNN NNN CCT GCA GGC TCG AG*T GCG GGA CGG CCA TCG GGA CCG GAG G digested with *Sbf*I and cloned into pUC18 (non-annealing nucleotides in italics, restriction sites underlined; all oligonucleotides were obtained by MWG, Ebersberg, Germany). The 500 bp downstream of the insertion site were amplified with *NNN NNC TCG AG*C CGC CCC AGC ACC GTT ACC ACC GAT AG and *NNN NNN NGG TAC C*CG CCG TGC TGA CCA GCC TAC, digested with *Xho*I and *Kpn*I and cloned into the product of the previous ligation to obtain the plasmid pUC18-UL35.

A linear DNA linker molecule providing an *Nco*I and a *Bsr*GI site was generated by annealing TCG ACC ATG GTG TAC AAC and TCG AGT TGT ACA CCA TGG, and ligated into the *Xho*I site of pUC18-UL35, resulting in pUC18-UL35NB. The fluorescent protein sequences from pEGFP-N1, pEYFP-N1 or pECFP-N1 (Clontech; Mountain View, CA) were excised with *Nco*I and *Bsr*GI and inserted into pUC18-UL35NB to generate pUC18-GFPUL35, -YFPUL35 or -CFPUL35. The complete constructs were amplified from these plasmids with ATG CCC GGC CGA TGA TGG and CGC CGT GCT GAC CAG CCT AC, and Red-recombination was used to replace the *rpsLneo* cassette of the bacterial artificial chromosome (BAC) pHSV1(17$^+$)blueLox-ΔVP26 (Fig. 1A; [8]). The resulting BACs were named pHSV1(17$^+$)blueLox-GFPVP26$_{\Delta aa\mathbf{5}-7}$, -YFPVP26-$_{\Delta aa\mathbf{5}-7}$, or -CFPVP26$_{\Delta aa\mathbf{5}-7}$, respectively (Fig. 1). From these BACs the modified UL35 ORFs were amplified, and the PCR products were sequenced (Seqlab; Göttingen, Germany). For transfection, BAC-DNA was prepared from 500 ml overnight *E. coli* cultures using the NucleoBond^{TM} BAC 100 kit (Macherey & Nagel; Düren, Germany). 5×10^5 Vero cells in 3.5 cm dishes were grown overnight, transfected with 2 µg BAC-DNA (MBS Mammalian Transfection Kit; Stratagene, La Jolla, CA), and cultured for several days until cytopathic effects developed.

Immunoblot

Vero cells grown to a density of 5.7×10^5 per 3.5 cm dish were synchronously infected with 10 plaque forming units (PFU)/cell in 500 µL for 2 h on ice, and then further cultured in regular growth medium at 37°C. After 1 h, the cells were washed for 3 min with citrate buffer (40 mM citric acid, pH 3, 135 mM NaCl, 10 mM KCl) to inactivate any extracellular virions that had not been internalized [60], and returned to fresh medium to initiate a synchronous infection. At different time points, the culture supernatants were collected and titrated. Infected cells and their complete supernatants were also harvested at 48 h post infection (p.i.). Viral particles released from infected cells into the culture medium were pelleted in a Beckman TLA100.3 rotor at 50,000 rpm for 30 min and resuspended in 100 µL hot SDS-PAGE sample buffer [61] with protease inhibitors. The cells were scraped into 200 µL of hot sample buffer with protease inhibitors and sheared by 50 passages through a 24 gauge needle. After SDS-PAGE on linear 5 to 15% polyacrylamide gradient gels and transfer onto a nitrocellulose membrane, viral proteins were probed with specific primary antibodies and alkaline-phosphatase-coupled secondary antibodies (Dianova; Hamburg, Germany).

Fluorescence Microscopy

Vero cells grown on cover slips to a density of 5 to 10×10^4 per 2 cm^2 were synchronously infected as described above at a multiplicity of infection (MOI) of 10 PFU/cell. At 9 h p.i., cells were fixed with 3% (w/v) para-formaldehyde (PFA) in PBS and permeabilized with 0.1% Triton X-100 (TX-100) for 5 min, fixed with absolute methanol, or fixed and permeabilized with PHEMO-fix (3.7% [w/v] PFA, 0.05% [w/v] glutaraldehyde, 0.5% [v/v] TX-100 in PHEMO buffer [68 mM PIPES, 25 mM HEPES, pH 6.9, 15 mM EGTA, 3 mM $MgCl_2$, 10% DMSO]) for 10 min. The HSV1 Fc receptor was blocked with 10% (v/v) human serum of healthy, HSV1-seronegative volunteers, and the samples were immunolabeled as described before [5,8,47,49,62,63]. All secondary antibodies were highly pre-adsorbed against cross-reactivities against other species than the intended one, and were coupled to lissamine-rhodaminesulfonyl chloride, RedX, fluorescein isothiocyanate, or Cy5 (Dianova, Hamburg, Germany). The cells were analyzed on an Axiovert 200M microscope equipped with a LSM 510 META confocal laser scanning unit (ZEISS, Jena, Germany) using a plan-apochromatic 63× oil-immersion objective with an 1.4 numeric aperture. Image acquisition and processing was performed using the ZEISS LSM imaging software, ImageJ 1.35 (Wayne Rasband; National Institute of Health, USA; http://rsb.info.nih.gov/ij/), and Adobe® Photoshop CS (Adobe Systems, San Jose, CA, USA). For classification and quantification of the intranuclear VP26 phenotype, we used a primary data set obtained from an analysis of at least 85 randomly chosen cells fixed at several time points from 4 to 12 h p.i. [8]. The degree of nuclear aggregate formation was classified based on the density and appearance of the anti-VP26 or GFPVP26 signals into the categories "none", "single", "grainy", and "aggregated".

Correlative Light and Electron Microscopy

RPE cells grown to 4×10^5 cells per 8.5 cm^2 on glass bottom dishes (MatTek Corporation, Ashland, MA, USA) with self-made marks to aid the localization of individual cells were synchronously infected with HSV1(KOS)-GFPVP26$_{\Delta aa\mathbf{1}-7}$ at an MOI of 10 PFU/cell. After 19.5 h of infection, the fluorescence signals were documented with a Zeiss Axiovert 200 microscope prior to fixation for 1 h at room temperature with 2% (w/v) glutaraldehyde in 130 mM cacodylate buffer at pH 7.4 containing 2 mM $CaCl_2$ and 10 mM $MgCl_2$. The cells were washed and further fixed and contrasted with 1% (w/v) OsO_4 in 165 mM cacodylate buffer at pH 7.4 containing 1.5% (w/v) $K_3Fe^{III}(CN)_6$ for 1 h followed by incubation in 0.5% (w/v) uranyl acetate in 50% (v/v) ethanol overnight. The cells were flat-embedded in Epon, and semi-thin sections cut parallel to the substrate were used to identify cells characterized by a high amount of nuclear aggregates and an indicative nuclear morphology that had been documented by epifluorescence microscopy prior to fixation. Such cells were then relocated in ultrathin sections of 50 nm and analyzed with a FEI Tecnai G2 T20 electron microscope. We analyzed ultrathin sections of more than 50 cells, and furthermore in detail by correlative light and electron microscopy 8 cells each containing more than 5 nuclear aggregates.

Results

Construction of HSV1 Strains with Tagged VP26

To identify strains whose capsid formation and intracellular trafficking mimic that of their untagged parent, we compared several constructs with different FP tags on VP26 that we had introduced into the HSV1(17$^+$)blueLox BAC. The

HSV1(17$^+$)blueLox-GFPVP26$_{\Delta aa1-7}$ strain, as the previously reported HSV1(KOS)-GFPVP26$_{\Delta aa1-7}$, lacks 65 bp upstream of the start codon of GFPVP26 including the seven N-terminal aa of VP26 (Fig. 1; P. Desai, personal communication and data not shown; [8,42]). Both strains propagate to similar titers in BHK cells [8].

In this study, we have generated the new strains HSV1(17$^+$)blueLox-CFPVP26$_{\Delta aa5-7}$, -GFPVP26$_{\Delta aa5-7}$, and -YFPVP26$_{\Delta aa5-7}$ (c.f. Fig. 1A, B) according to a strategy originally described by Desai & Person (1998). The codons for aa 5 to 7 of VP26 were replaced by different FPs with the linkers His-Ser-Thr and Asn-Ser-Ser at their respective N- and C-termini (Fig. 1B). The viral genomes of these strains contained the engineered changes in UL35 (arrowheads in Fig. 2A) but not any major unwanted alterations as shown by restriction enzyme digestion with *Not*I, *Eco*RI, *Eco*RV or *Sbf*I (Fig. 2A and data not shown). There was some heterogeneity among strains in the *Not*I joint fragments around 3.3 kb (asterisks in Fig. 2A) that do not seem to have any influence on infectivity as reported previously [8,63,64]. Sequencing the UL35 region of the BACs confirmed the correct insertion of the FP sequences (not shown). But after transfection of Vero cells with these BACs, unexpectedly only pHSV1(17$^+$)blueLox-CFPVP26$_{\Delta aa5-7}$ gave rise to regular fluorescent plaques, whereas -GFPVP26$_{\Delta aa5-7}$ yielded tiny plaques, and -YFPVP26$_{\Delta aa5-7}$ merely single fluorescent cells (data not shown). So, surprisingly the four additional aa derived from the authentic VP26 N-terminus, the three linker aa His-Ser-Thr or maintaining the authentic non-coding 50 bp upstream sequences inhibited replication of pHSV1(17$^+$)blueLox-GFPVP26$_{\Delta aa5-7}$ and -YFPVP26$_{\Delta aa5-7}$, but not that of pHSV1(17$^+$)blueLox-CFPVP26$_{\Delta aa5-7}$.

To further characterize potential differences between these strains, we compared their growth kinetics and protein expression. While HSV1(17$^+$)blueLox-ΔVP26 and -mRFPVP26$_{\Delta aa1-7}$ were attenuated in BHK cells [8], there was no growth difference between HSV1(17$^+$)blueLox, -ΔVP26 and -mRFPVP26$_{\Delta aa1-7}$ in Vero cells (Fig. 2B). But compared to those, -CFPVP26$_{\Delta aa5-7}$ and -GFPVP26$_{\Delta aa1-7}$ were slightly attenuated, and -GFPVP26$_{\Delta aa1-7}$ replicated with delayed kinetics (Fig. 2B). Likewise, HSV1(17$^+$)blueLox-GFPVP26$_{\Delta aa1-7}$ is delayed in BHK cells when compared to -mRFPVP26$_{\Delta aa1-7}$ [8]. Thus, the growth properties of these HSV1 strains varied depending on the type of the tag, the location of the tag, and the cell line. After synchronous infection of Vero cells with an MOI of 10 PFU/cell (Fig. 2C), the parental HSV1(17$^+$) synthesized more proteins and secreted more virions into the medium than HSV1(17$^+$)blueLox and its derivatives. An antibody raised against VP26 detected a band around 12 kDa after infection with HSV1(17$^+$) or HSV1(17$^+$)blueLox but not with HSV1(17$^+$)blueLox-ΔVP26. After infection with the tagged strains, there was one major band at 38 kDa for -CFPVP26$_{\Delta aa5-7}$ or -GFPVP26$_{\Delta aa1-7}$ in addition to some other minor bands. mRFPVP26$_{\Delta aa1-7}$ had a higher apparent molecular weight, although mRFP is about 1 kDa smaller than GFP. More of the CFPVP26$_{\Delta aa5-7}$ fusion protein was synthesized when compared to GFPVP26$_{\Delta aa1-7}$ or mRFPVP26$_{\Delta aa1-7}$, possibly due to upstream promoter elements that were missing in the latter two strains (c.f. Fig. 1B). These data show furthermore that all VP26 fusion proteins of the infectious HSV1 strains were incorporated into secreted virions as full-length proteins.

Nuclear Aggregates Induced by HSV1-XFPVP26 Impair Nuclear Capsid Egress

To assess the influence of VP26 tagging on virus assembly, we infected Vero cells with 10 PFU/cell for 9 h, by which time many wild type capsids have left the nucleus but not the cells [8,63], and analyzed them by confocal fluorescence microscopy. After infection with HSV1(17$^+$)blueLox (Fig. 3A, wild type), -mRFPVP26$_{\Delta aa1-7}$ (Fig. 3B), or -GFPVP26$_{\Delta aa1-7}$ (Fig. 3C), nuclear and cytoplasmic capsids labeled by antibodies against VP26 or VP5 were also highlighted by mRFP or GFP in the respective strains. The signals for nuclear mRFPVP26$_{\Delta aa1-7}$ and GFPVP26$_{\Delta aa1-7}$ were similar or weaker than those of anti-VP5 (Fig. 3B/Cii) and anti-VP26 (Fig. 3B/Ciii). In contrast, more cytoplasmic capsids (arrows in Fig. 3A–C) were detected by mRFPVP26$_{\Delta aa1-7}$ (Fig. 3Bi) or GFPVP26$_{\Delta aa1-7}$ (Fig. 3Ci) than by the antibodies. However, HSV1(17$^+$)blueLox-GFPVP26$_{\Delta aa1-7}$ but not -mRFPVP26$_{\Delta aa1-7}$ or HSV1 wild type also induced the formation of large nuclear GFP aggregates that also contained VP5 and VP26 (Fig. 3C). Furthermore, there were fewer cytoplasmic capsids after infection with HSV1(17$^+$)blueLox-GFPVP26$_{\Delta aa1-7}$ than with -mRFPVP26$_{\Delta aa1-7}$. Later during infection, HSV1(17$^+$)blueLox and -mRFPVP26$_{\Delta aa1-7}$ also induced such nuclear aggregates (not shown). Notably, in other cell lines such as HeLa cells, RPE cells or primary neurons, the nuclear aggregates of HSV1(17$^+$)blueLox-GFPVP26$_{\Delta aa1-7}$ were even more prominent than in Vero cells, but -mRFPVP26$_{\Delta aa1-7}$ always induced fewer aggregates (not shown).

As described above, transfection with the BACs pHSV1(17$^+$)blueLox-GFPVP26$_{\Delta aa5-7}$ or -YFPVP26$_{\Delta aa5-7}$ did not yield virions. But an analysis of transfected cells revealed small nuclear GFPVP26$_{\Delta aa5-7}$ flecks of the typical capsid size as well as large nuclear GFPVP26$_{\Delta aa5-7}$ aggregates, which were both also labeled by antibodies against VP5 or VP26 (Fig. 3D). However, there were much fewer cytoplasmic GFPVP26$_{\Delta aa5-7}$ capsids than after infection with HSV1(17$^+$)blueLox-GFPVP26$_{\Delta aa1-7}$ (c.f. Fig. 3C with Fig. 3D). The nuclear aggregates after transfection with -YFPVP26$_{\Delta aa5-7}$ were even larger and of irregular shape, and there were no individual nuclear or cytoplasmic capsids (data not shown). In contrast, the strain HSV1(17$^+$)blueLox-CFPVP26$_{\Delta aa5-7}$ induced fewer and smaller nuclear aggregates, and there were single nuclear and cytoplasmic capsids, both after transfection and infection (not shown). The difference between HSV1(17$^+$)blueLox-GFPVP26$_{\Delta aa1-7}$ and -GFPVP26$_{\Delta aa5-7}$ might have been due to different expression levels as the protein GFPVP26$_{\Delta aa1-7}$ had been expressed from viral genomes, whereas the mRNAs for GFPVP26$_{\Delta aa5-7}$ were transcribed from the transfected BAC plasmids. However, in the case of HSV1(17$^+$)blueLox-GFPVP26$_{\Delta aa1-7}$, capsids were exported to the cytoplasm after both, infection for 9 h (Fig. 3C), or transfection for 24 h (Fig. 3E). While GFPVP26$_{\Delta aa5-7}$ was largely confined to the nucleus (Fig. 3Di), GFPVP26$_{\Delta aa1-7}$ particles even spread from the transfected to neighboring cells and were transported to the neighboring nucleus (Fig. 3Ei, white arrows). After PHEMO fixation, DNA could be detected in the nuclear aggregates by TO-PRO-3 staining, whereas after PFA fixation this was not the case (Fig. 3Eiii) as described previously [4].

We have reported previously that the capsids of HSV1(17$^+$)blueLox accumulate faster in the cytoplasm than those of HSV1(17$^+$)blueLox-GFPVP26$_{\Delta aa1-7}$-gDmRFP (Fig. 8C in [8]). Here, we have analyzed also the time course of nuclear aggregate formation using the same data set of randomly collected confocal fluorescence microscopy images. The cells were classified by their phenotypes as having (i) no nuclear VP26 as in uninfected cells (none), (ii) individual nuclear capsids (single), (iii) many capsids filling the entire nucleus (grainy), or (iv) nuclear aggregates containing VP26 (Fig. 4A). Already 4 h after infection with HSV1(17$^+$)blueLox (Fig. 4B), more than 30% of the cells contained nuclear capsids, and by 8 h almost 90% of the nuclei

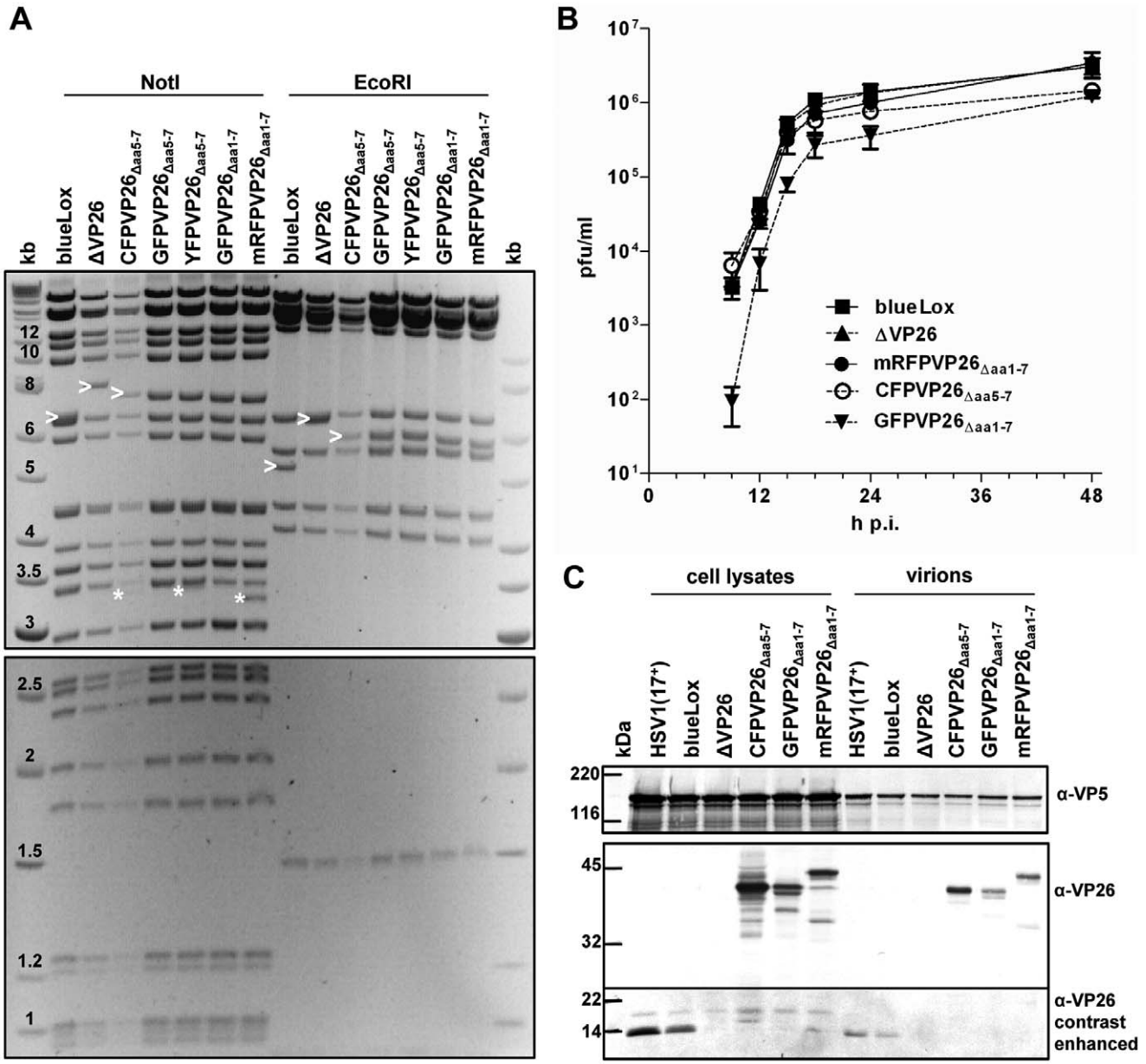

Figure 2. Characterization of HSV1(17$^+$)blueLox-VP26 strains. (A) Restriction digestion analysis of different BAC clones with *Not*I and *Eco*RI. Band shifts resulting from modifications in the UL35 ORF (arrowheads) and the *Not*I joint fragments containing the viral a-sequences (asterisks) are indicated. DNA sizes in kb. (B) For single-step growth kinetics, Vero cells were infected in duplicates with 10 PFU/cell, and the amount of secreted infectious virus at a given time point was determined by duplicate plaque assays. (C) Vero cells were infected at an MOI of 10 PFU/cell with HSV1(17$^+$) or HSV1(17$^+$)blueLox and its derivatives as indicated. After 48 h, the cells and virions secreted into the culture medium were harvested, and analyzed by SDS-PAGE and immunoblotting for expression of VP5 (α-NC-1) and VP26 (α-VP26). The signals in the molecular weight range below 25 kDa were further contrast enhanced.
doi:10.1371/journal.pone.0044177.g002

contained many nuclear capsids. By 12 h, the first nuclear aggregates appeared in the nuclei of some few cells. In contrast, after infection with HSV1(17$^+$)blueLox-GFPVP26$_{\Delta aa\mathbf{1}-7}$-gDmRFP (Fig. 4C), there were already prominent nuclear aggregates in 25% of the nuclei after 6 h, and by 10 h this had risen to 70% [8]. In summary, our data indicate an inverse correlation between the amount of nuclear aggregate formation and the efficiency of nuclear capsid egress and thus infectivity. The extent of inhibition depended on the type of the tag with mRFP or CFP being almost non-invasive, on the location of the tag with XFPVP26$_{\Delta aa\mathbf{1}-7}$ being better tolerated than XFPVP26$_{\Delta aa\mathbf{5}-7}$, and on the cell line with Vero cells being less prone to aggregate formation than HeLa, RPE or neuronal cells.

Nuclear Aggregates Contain Capsid Proteins but not Capsids

To further characterize the protein composition of the aggregates, we determined the subcellular localization of other HSV1 proteins in infected or transfected Vero cells (summarized

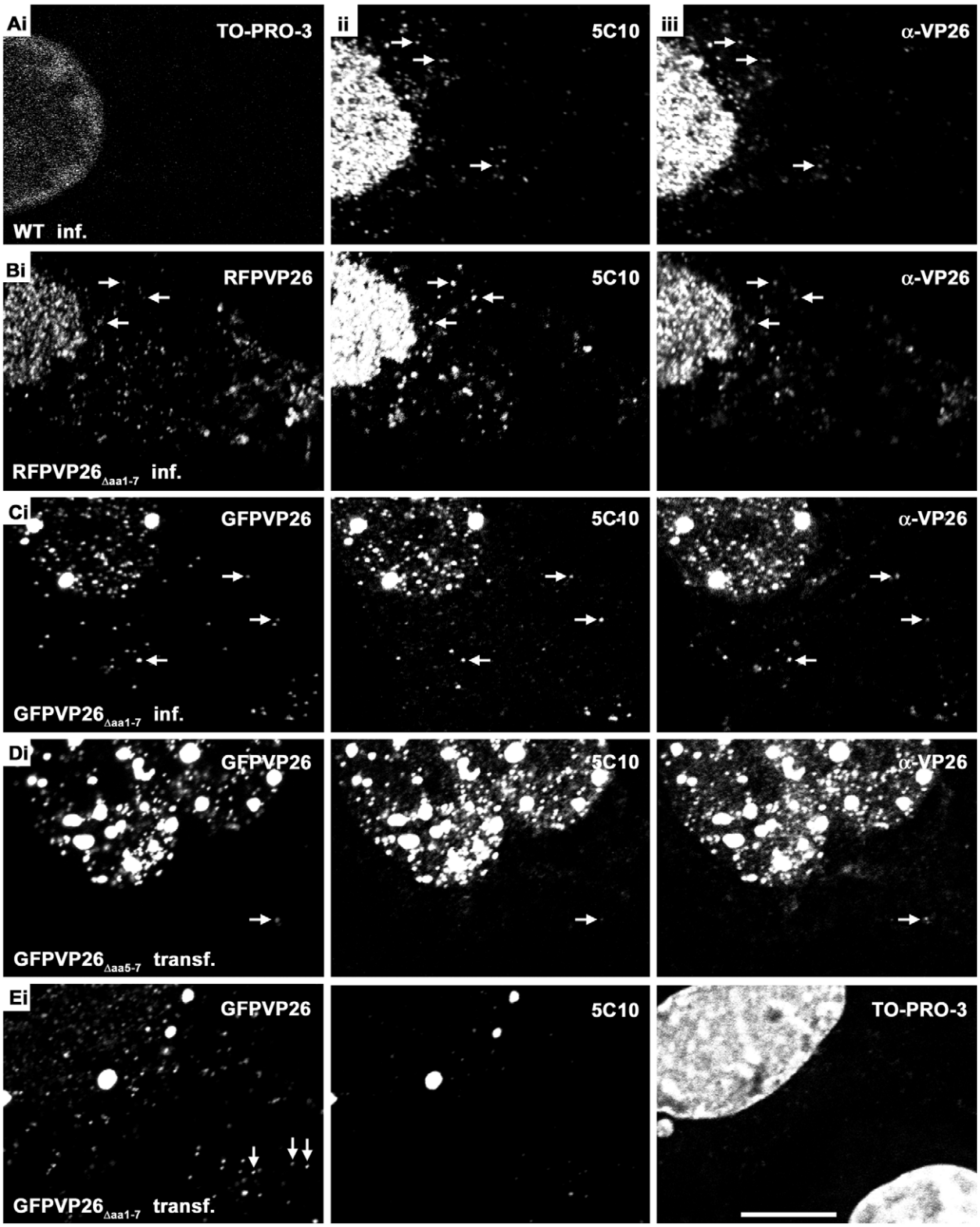

Figure 3. Nuclear aggregates induced by HSV1-XFPVP26 impair nuclear capsid egress. Vero cells were infected (inf.) with 10 PFU/cell of HSV1(17^{+})blueLox (A, wild type), HSV1(17^{+})blueLox-mRFPVP26$_{\Delta aa\mathbf{1}-7}$ (B), or HSV1(17^{+})blueLox-GFPVP26$_{\Delta aa\mathbf{1}-7}$(C), and fixed at 9 h with PFA. Alternatively, cells were transfected (transf.) with pHSV1(17^{+})blueLox-GFPVP26$_{\Delta aa\mathbf{5}-7}$ (D) or pHSV1(17^{+})blueLox-GFPVP26$_{\Delta aa\mathbf{1}-7}$ (E), and fixed at 24 h. In addition to the intrinsic fluorescence of the XFPVP26 constructs (mRFPVP26 or GFPVP26), the subcellular localization of VP26 (α-VP26) and VP5 (MAb 5C10) were analyzed after permeabilization with TX-100 and immunolabeling by confocal fluorescence microscopy. The nuclei were stained with TO-PRO-3 (A, E). Arrows highlight cytoplasmic capsids (A–D) or incoming capsids at the nuclear rim of a neighboring cell (Ei). Scale bar: 10 μm.
doi:10.1371/journal.pone.0044177.g003

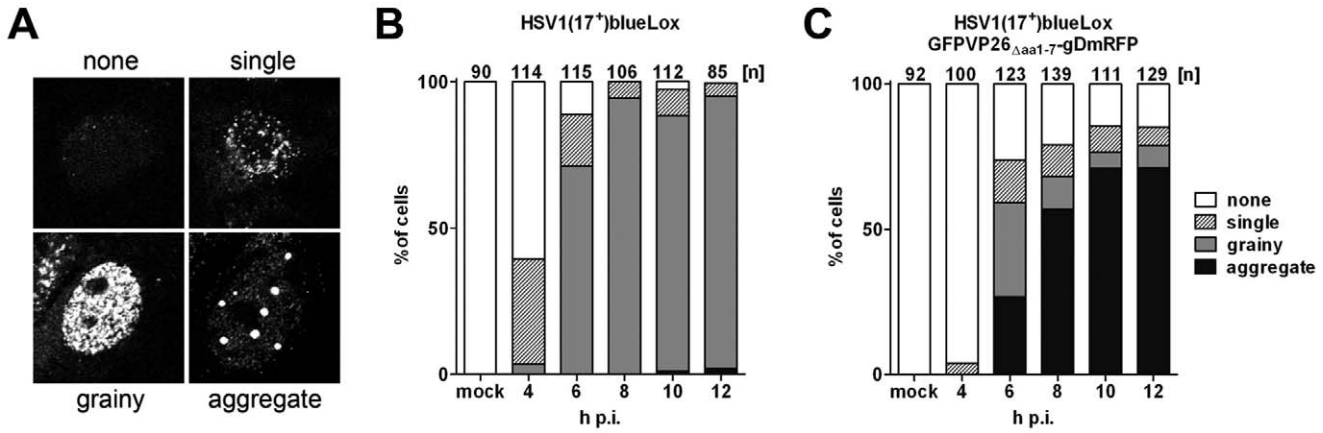

Figure 4. Quantification of nuclear aggregate formation. Vero cells were infected with 10 PFU/cell of HSV1(17$^+$)blueLox (B) or HSV1(17$^+$)blueLox-GFPVP26$_{\Delta aa\mathbf{1}-7}$-gDmRFP (C), and the cells were fixed at 4, 6, 8, 10, or 12 h. After permeabilization, HSV1(17$^+$)blueLox infected cells were labeled with an antibody directed against VP26. According to their intranuclear VP26 phenotype, the cells were classified into "none", "single", "grainy" and "aggregate" (A). The numbers above the columns describe the number of nuclei analyzed for each time point.
doi:10.1371/journal.pone.0044177.g004

in Table 1). Antibodies against two minor capsid associated proteins, pUL25 (Fig. 5Aiii) or pUL17 (Fig. 5Bii), as well as VP26 (Fig. 5Biii, 5Ciii, 5Diii), co-localized with the XFPVP26 throughout the nuclear aggregates, both after infection with HSV1(17$^+$)blueLox-GFPVP26$_{\Delta aa\mathbf{1}-7}$ (Fig. 5A-D), or after transfection with pHSV1(17$^+$)blueLox-GFPVP26$_{\Delta aa\mathbf{5}-7}$ (Fig. 5E). The MAb 5C10 directed against mature hexon epitopes also highlighted the entire volume of the aggregates(Fig. 5Aii, 3Cii, 3Dii, 3Eii), while MAb 8F5, also recognizing mature hexon epitopes, was enriched on the periphery of the aggregates (Fig. 5Cii, 5Dii, 5Fii). Since de Oliveira et al. (2008) detected a high amount of XFPVP26 on the periphery of the aggregates [4], we also imaged them with less sensitive detection settings at higher magnification (Fig. 5D). Occasionally, large aggregates appeared to consist of smaller entities but the GFPVP26 or anti-VP26 signals did not seem to be particularly enriched on the rims of the aggregates (Fig. 5Di and 5Diii). Nevertheless, MAb LP12 and MAb H1.4, two other antibodies directed against VP5, also preferentially labeled the periphery but not the center of most aggregates (not shown; summarized in Table 1). Surprisingly, in cells transfected with pHSV1(17$^+$)blueLox-GFPVP26$_{\Delta aa\mathbf{5}-7}$, the mature hexon epitope recognized by MAb 8F5 was not detected at all (Fig. 5Eii), whereas the other antibodies directed against VP5 resulted in similar patterns as after infection with HSV1(17$^+$)blueLox-GFPVP26$_{\Delta aa\mathbf{1}-7}$ (summarized in Table 1). This was not due to different expression levels in infected or transfected cells, as the MAb 8F5 epitope was formed after both, infection or transfection with pHSV1(17$^+$)blueLox-GFPVP26$_{\Delta aa\mathbf{1}-7}$ (Fig. 5Fii).

Using correlative light and electron microscopy, we further analyzed RPE cells after infection with HSV1(KOS)-GFPVP26$_{\Delta aa\mathbf{1}-7}$ (Fig. 6), a virus-cell combination that was particularly prone to nuclear aggregate formation. Prior to fixation, the subcellular localization of the nuclear aggregates was documented by fluorescence microscopy (Fig. 6A). Corresponding electron micrographs of ultrathin sections through such cells showed (Fig. 6B), particularly at higher magnifications (Fig. 6C–E) that these aggregates contained amorphous electron dense material (arrows) but no capsids, and that capsids (arrowheads) were found rarely at the periphery of the aggregates. The aggregates reacted specifically with the uranyl acetate stain that is applied after sectioning for contrast, indicating that this material was rich in proteins and/or nucleic acids (data not shown). The different types of A, B, and C capsids had all been generated, and sometimes also clustered into larger assemblies (Fig. 6C and E, arrowheads). In summary, immune labeling, the TO-PRO-3 staining after PHEMO fixation (not shown), and the electron microscopy analysis demonstrated that the nuclear aggregates comprised most, if not all capsid proteins and DNA, but many of them only abut HSV1 capsids, and the MAb 8F5 epitope was only formed on the aggregate periphery, or not at all after transfection with pHSV1-GFPVP26$_{\Delta aa\mathbf{5}-7}$.

Nuclear Aggregates do not Sequester pUL36, pUS3 or pUL34 and are Neither Replication Compartments nor Promyelocytic Leukemia Protein Nuclear Bodies

Like pUL17 and pUL25, the large inner tegument protein pUL36 has also been implicated in nuclear capsid egress [65–67]. After infection with HSV1(17$^+$)blueLox (Fig. 7A) or HSV1(17$^+$)blueLox-GFPVP26$_{\Delta aa\mathbf{1}-7}$ (Fig. 7B), pUL36 as detected by antibodies raised against a middle region (pUL36$_{aa1408-2112}$) or its C-terminus (pUL36$_{aa3048-3057}$; not shown) was enriched in the perinuclear cytoplasm and localized in the cell periphery, where it co-localized with VP5 (arrows in Fig. 7Aii and 7Aiii), as reported previously [63]. The host chromatin, stained with TO-PRO-3, was marginalized to the nuclear periphery (Fig. 7Ai), as reported previously [68]. pUL36 did not colocalize with nuclear aggregates after infection with HSV1(17$^+$)blueLox-GFPVP26$_{\Delta aa\mathbf{1}-7}$ (7Biii). After transfection with pHSV1(17$^+$)blueLox-GFPVP26$_{\Delta aa\mathbf{5}-7}$ that does not release capsids from the nucleus into the cytoplasm (Fig. 7Ci), pUL36 was similarly distributed in the cytoplasm (Fig. 7Ciii). In few cells transfected with pHSV1(17$^+$)blueLox-GFPVP26$_{\Delta aa\mathbf{5}-7}$, pUL36 was enriched on the periphery of the nuclear aggregates (Fig. 7Ciii). In contrast, the HSV1 protein kinase pUS3 and the integral membrane protein pUL34 that function in nuclear capsid egress (reviewed in [66,67] were localized at the nuclear envelope as after infection with HSV1 wild type, and not redirected to the nuclear aggregates (not shown).

The morphology of the nuclear aggregates seemed to have some resemblance to nuclear DNA replication compartments [69–71]. After infection with HSV1(17$^+$)blueLox, the single-strand DNA binding protein ICP8, an essential component of the HSV1

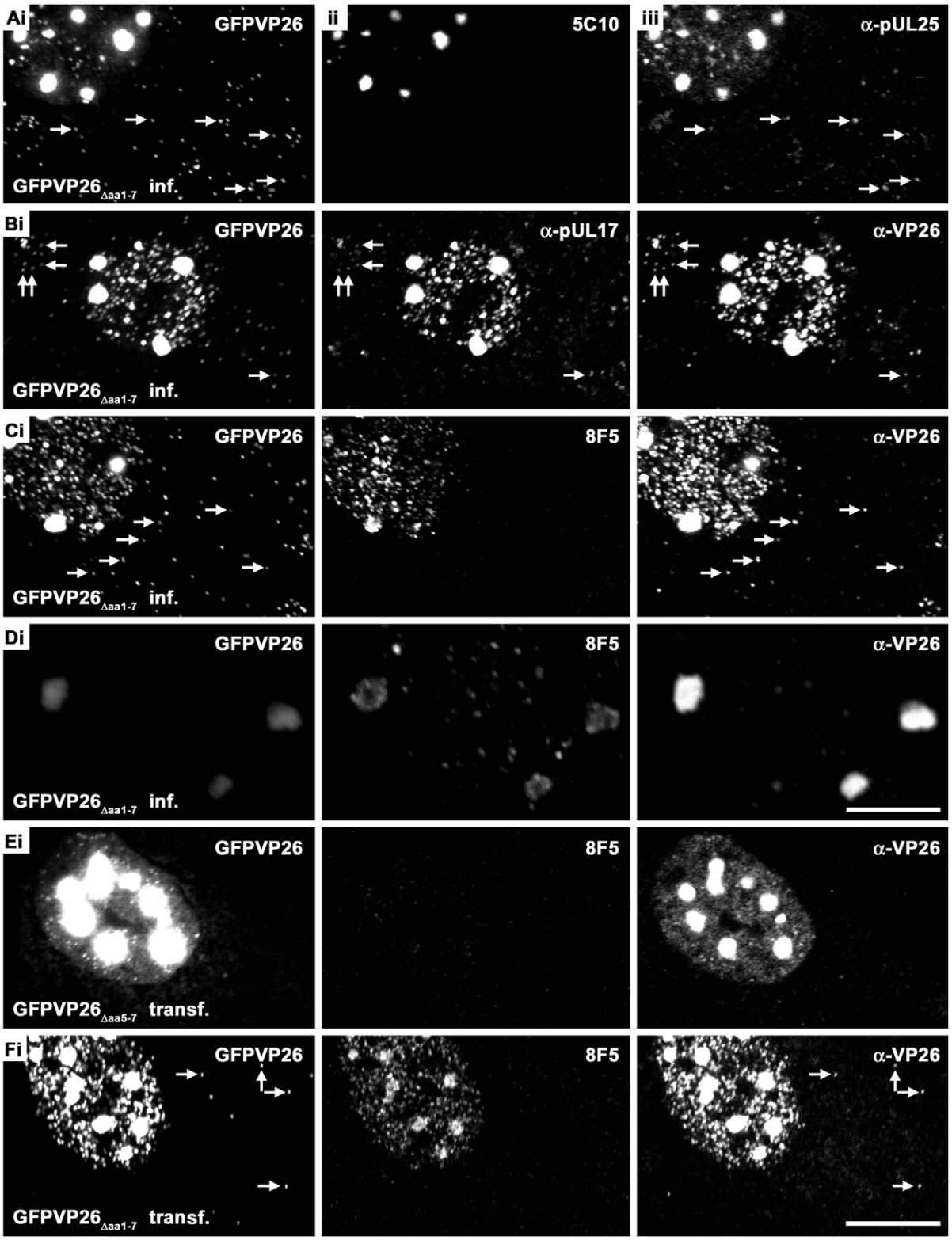

Figure 5. Nuclear aggregates contain capsid proteins. Vero cells were infected (inf.) with 10 PFU/cell of HSV1(17^{+})blueLox-GFPVP26$_{\Delta aa\mathbf{1}-7}$ for 9 h (A–D) or transfected (transf.) with pHSV1(17^{+})blueLox-GFPVP26$_{\Delta aa\mathbf{5}-7}$ (E) or pHSV1(17^{+})blueLox-GFPVP26$_{\Delta aa\mathbf{1}-7}$ (F) for 24 h. The cells were fixed with PFA and permeabilized with TX-100. GFPVP26 was detected by its intrinsic fluorescence (left column). Furthermore, the cells were labeled with different VP5 antibodies (MAb 8F5 or 5C10) and with α-VP26, α-pUL25 or α-pUL17, and analyzed by confocal fluorescence microscopy. For row D, the specimen was scanned at higher magnification and lower photomultiplier settings. The arrows point to cytoplasmic capsids. Bars: 5 μm (D), 10 μm (F).

doi:10.1371/journal.pone.0044177.g005

Table 1. Characterization of HSV1-GFPVP26 nuclear aggregates.

Antigen	Antibody	HSV1(17$^+$)blueLox- GFPVP26	Subcellular localization	Detection in nuclear aggregates	
VP26	pAb aa 95–112	Δaa**1**–7 infection	mainly nuclear,	+++	entire
		Δaa**5**–7 transfection	cytoplasmic dots		
VP5	mAb5C10	Δaa**1**–7 infection	mainly nuclear,	+++	entire
		Δaa**5**–7 transfection	cytoplasmic dots		
	mAb 8F5	Δaa**1**–7 infection	mainly nuclear,	++	periphery
		Δaa**1**–7 transfection	cytoplasmic dots		
		Δaa**5**–7 transfection	epitope not formed	–	–
	mAb H1.4	Δaa**1**–7 infection	mainly nuclear,	++	periphery
		Δaa**5**–7 transfection	cytoplasmic dots		
	mAb LP12	Δaa**1**–7 infection	mainly nuclear,	++	periphery
		Δaa**5**–7 transfection	cytoplasmic dots		
VP22a	pAb NC-3,4	Δaa**1**–7 infection	mainly nuclear,	- (PFA)	periphery
			cytoplasmic dots	+++ (MeOH)	
				+ (PHEMO)	
		Δaa**5**–7 transfection		++ (PHEMO)	periphery
VP23	pAb NC-5	Δaa**1**–7 infection	nuclear, nuclear rim,	–	–
		Δaa**5**–7 transfection	perinuclear region		
	mAb 1D2	Δaa**1**–7 infection	nuclear rim	–	–
		Δaa**5**–7 transfection			
pUL25	mAb ID1,	Δaa**1**–7 infection	mainly nuclear,	+++	entire
	pAb#166	Δaa**5**–7 transfection	cytoplasmic dots		
pUL17	pAb #203	Δaa**1**–7 infection	mainly nuclear,	+++	entire
	aa 154-703	Δaa**5**–7 transfection	cytoplasmic dots		
light capsid	pAb anti-LC	Δaa**1**–7 infection	mainly nuclear,	+++	periphery
		Δaa**5**–7 transfection	cytoplasmic dots		
pUL36	pAb #147	Δaa**1**–7 infection	mainly perinuclear,	–	–
	aa 1408–2112	Δaa**5**–7 transfection	cytoplasm	+	periphery
	pAb C-term	Δaa**1**–7 infection	mainly perinuclear,	–	–
	aa 3048–3057	Δaa**5**–7 transfection	cytoplasm	+	periphery
pUS3	pAb aa 98–364	Δaa**1**–7 infection	nuclear, nuclear rim,	–	–
		Δaa**5**–7 transfection	perinuclear region		
pUL34	pAb aa 1–252	Δaa**1**–7 infection	mainly nuclear rim	–	–
		Δaa**5**–7 transfection			
ICP8	mAb HB8180	Δaa**1**–7 infection	nuclear	–	–
		Δaa**5**–7 transfection			
PML	pAb H-238	Δaa**1**–7 infection	degraded	–	–
	aa157–394	Δaa**5**–7 transfection			

Vero cells were infected with HSV1(17$^+$)blueLox-GFPVP26$_{\Delta aa\mathbf{1}–7}$ at an MOI of 10 PFU/cell and fixed at 9 h, or transfected with pHSV1(17$^+$)blueLox-GFPVP26$_{\Delta aa\mathbf{5}–7}$ or -GFPVP26$_{\Delta aa\mathbf{1}–7}$ and fixed at 24 h. The cells had been fixed with PFA unless indicated otherwise, and subsequently labeled with different antibodies. MeOH, methanol fixation; PHEMO, PHEMO fixation; –, not detected.

doi:10.1371/journal.pone.0044177.t001

replication machinery, and GFPVP26 occupied very similar nuclear regions as reported previously [72]. Higher resolution showed that ICP8 and capsid proteins did not co-localize although they were located very close to each other (not shown). Also after infection with HSV1(17$^+$)blueLox-GFPVP26$_{\Delta aa\mathbf{1}–7}$ (Fig. 7D) or transfection with pHSV1(17$^+$)blueLox-GFPVP26$_{\Delta aa\mathbf{5}–7}$ (Fig. 7E), ICP8 was not targeted to the nuclear aggregates. The SCP of VZV interacts with a promyelocytic leukemia protein, a component of nuclear promyelocytic leukemia protein bodies that sequester progeny VZV capsids and thus reduce virion formation [73,74]. We therefore tested whether the nuclear HSV1 aggregates or capsids might have been trapped by this intrinsic antiviral defense mechanism. However, while uninfected cells contain several ND10 domains in each nucleus, the promyelocytic leukemia protein bodies were degraded after infection with HSV1(17$^+$)blueLox-GFPVP26$_{\Delta aa\mathbf{1}–7}$ as well as with HSV1(17$^+$)blueLox (not shown), as reported before for HSV1 wild type [75]. Therefore, the nuclear aggregates do not represent anti-viral promyelocytic leukemia protein bodies.

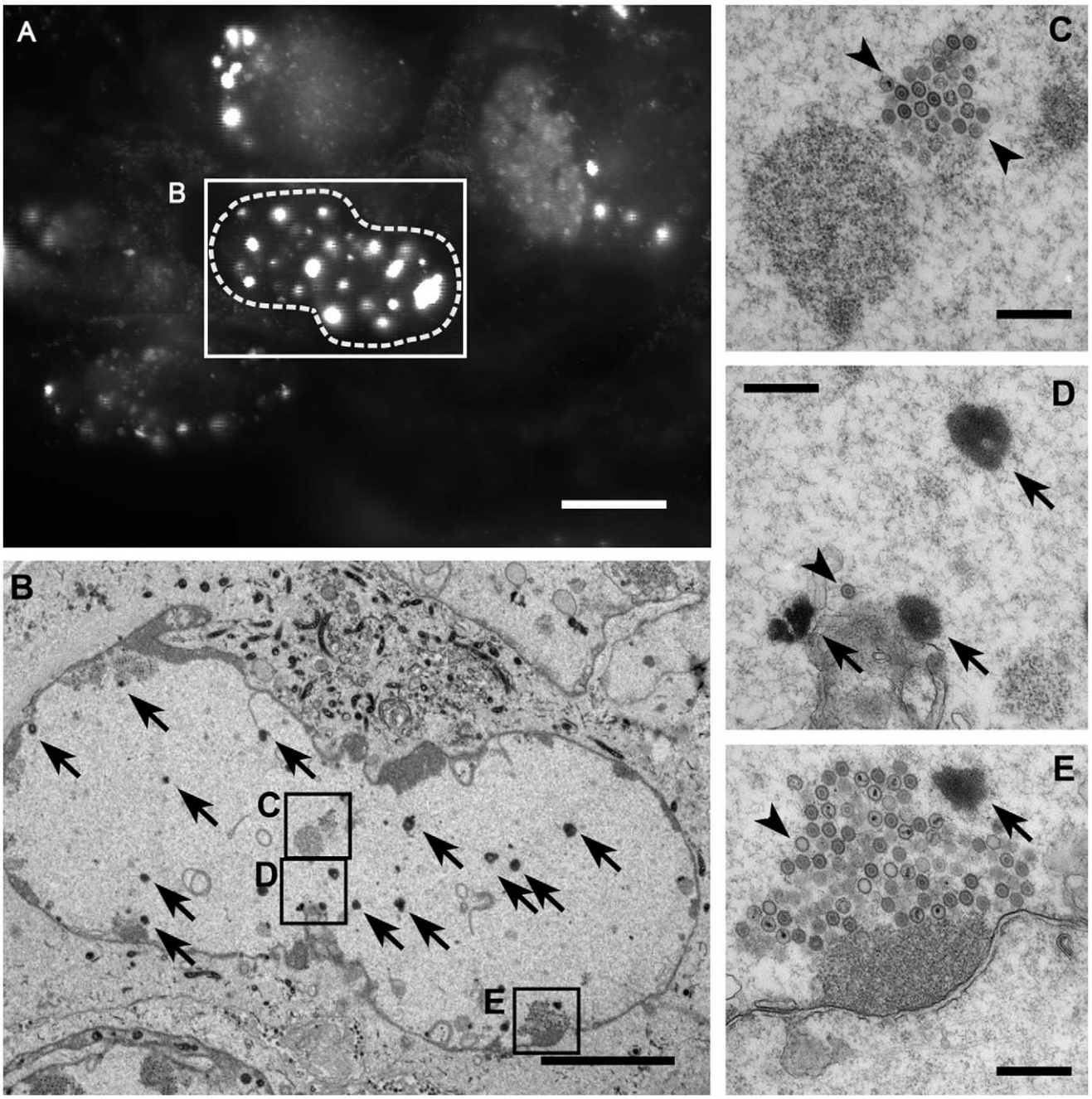

Figure 6. Nuclear aggregates do not contain capsids. RPE cells were infected with HSV1(KOS)-GFPVP26$_{\Delta aa1-7}$ at an MOI of 10 PFU/cell. At 19.5 h, the cells were analyzed by fluorescence microscopy to identify nuclei with bright fluorescence spots (A). After fixation, embedding and sectioning these cells were further analyzed by electron microscopy (B–E). The nuclei contain nuclear capsids (arrowheads) as well as the amorphous electron dense material representing the aggregates (arrows) identified by fluorescence microscopy. The aggregates do not contain capsids (arrowheads). Bars: 10 μm (A), 5 μm (B), and 500 nm (C–E).
doi:10.1371/journal.pone.0044177.g006

Discussion

Tagging of HSV1-VP26

Our attempts to tag the N-terminus of the non-essential small capsid protein VP26 of HSV1(17$^+$)blueLox revealed that subtle differences in the FP domain defined whether a transfected BAC replicated with wild type kinetics or was non-infectious (c.f. Fig. 1). The degree of nuclear aggregate formation correlated with an impediment of nuclear capsid egress and depended on the presence of upstream non-coding sequences, the tag with mRFP or CFP being less invasive than GFP or YFP, the location of the tag with XFPVP26$_{\Delta aa1-7}$ being better tolerated than XFPVP26$_{\Delta aa5-7}$, and the cell type with Vero cells generating fewer aggregates than HeLa, RPE or primary neurons.

In cells infected with HSV1(17$^+$), immunolabeling for VP5 or VP26 does not reveal such nuclear aggregates up to 15 h p.i., but rather results in a grainy pattern that most likely represents individual capsids (Fig. 3A; 4B; 7A; [62,63]). Notably, release of

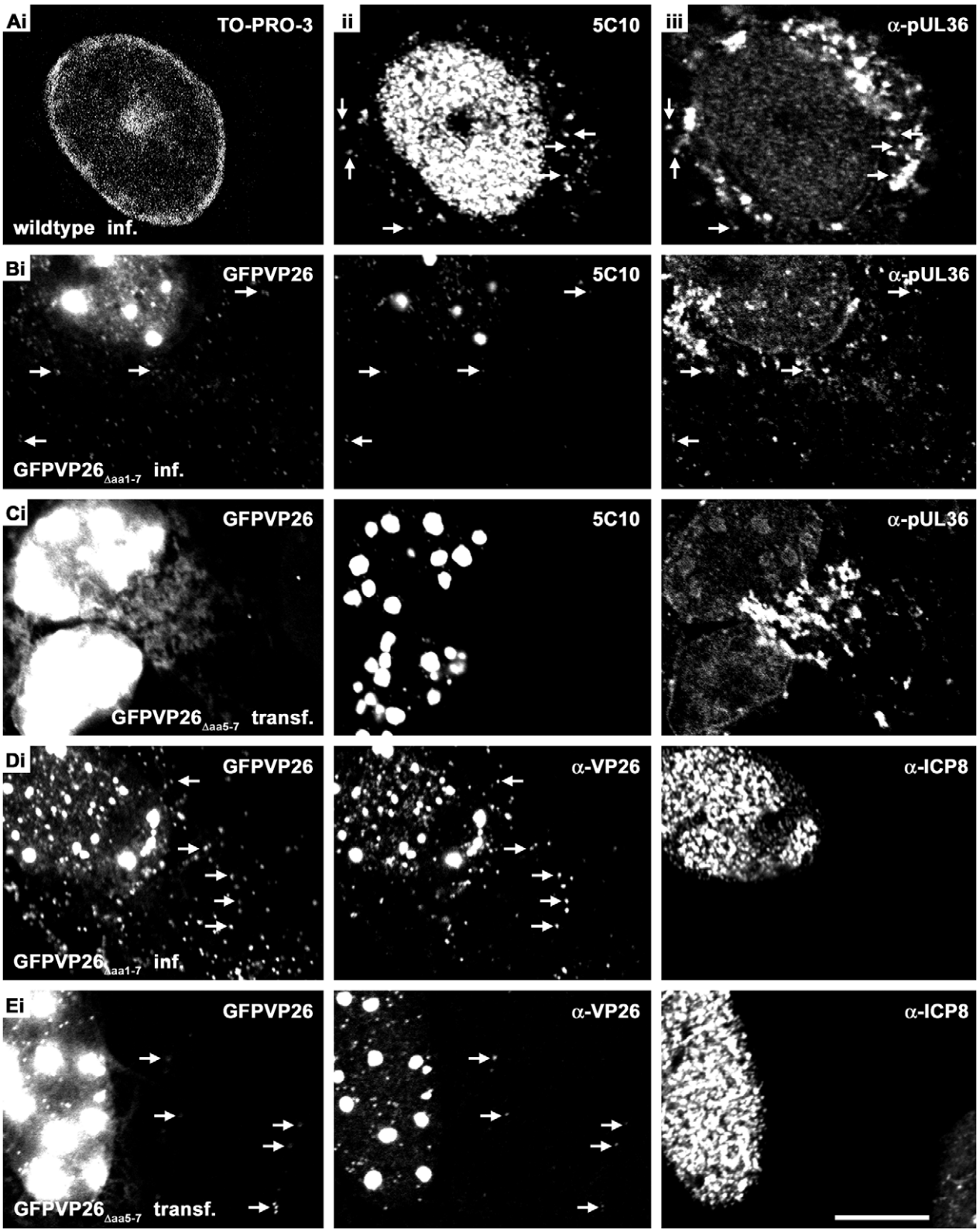

Figure 7. Nuclear GFPVP26 aggregates do not sequester pUL36 and are not DNA replication compartments. Vero cells were infected (inf.) for 9 h with 10 PFU/cell of HSV1(17^{+})blueLox (A) or HSV1(17^{+})blueLox-GFPVP26$_{\Delta aa\mathbf{1}-7}$ (B, D), or transfected (transf.) with the pHSV1(17^{+})blueLox-GFPVP26$_{\Delta aa\mathbf{5}-7}$ for 24 h(C, E). The cells were fixed with PFA and permeabilized with TX-100. GFPVP26 was detected by its intrinsic fluorescence. Furthermore, the cells were labeled with anti-pUL36$_{aa1408-2112}$ and with MAb 5C10 against VP5 (A–C), against the single-strand DNA binding protein ICP8 and VP26 (D, E), or with TO-PRO-3 to stain the DNA (A). The arrows point to cytoplasmic capsids. Scale bar: 10 μm.
doi:10.1371/journal.pone.0044177.g007

infectious particles from the infected cells commences as early as 12 h p.i. (Fig. 2B; [8]). Therefore, we consider the nuclear VP26 aggregates that formed with certain FP tags as early as 6 h p.i. to be non-physiological. Since the subcellular distribution of mRFPVP26$_{\Delta aa\mathbf{1}-7}$ resembles that of the authentic VP26 more closely than the GFP variants, HSV1-mRFPVP26$_{\Delta aa\mathbf{1}-7}$ strain seems best suited to investigate the assembly and intracellular trafficking of HSV1.

The distinct phenotypes of the FPVP26 constructs may be related to differences in their quaternary structure. While GFP and YFP tend to dimerize with dissociation constants around 0.1 mM, the N146I mutation in CFP does not only increase its brightness but also its dissociation constant to 3 mM [76–79]. mRFP is not related to GFP and has been designed to remain monomeric [80]. Thus, dimerization and aggregate induction of GFPVP26$_{\Delta aa\mathbf{5}-7}$ and YFPVP26$_{\Delta aa\mathbf{5}-7}$ may be favored when compared to CFPVP26$_{\Delta aa\mathbf{5}-7}$ and mRFPVP26$_{\Delta aa\mathbf{1}-7}$, given the high concentration of capsid proteins in the nucleoplasm, and given an intrinsic dissociation constant of 0.02 mM for recombinant VP26 [28]. Furthermore, deleting non-coding sequences upstream of the UL35 gene reduced expression, and thus possibly the toxicity of GFPVP26$_{\Delta aa\mathbf{1}-7}$ when compared to GFPVP26$_{\Delta aa\mathbf{5}-7}$. Indeed, these 50 bp encompass a sequence with perfect consensus to the Inr element YYANWYY required for efficient transcription from HSV1 late promoters [81]. Another similar sequence within the deletion and two other sequences upstream of the deletion diverge from the Inr consensus in the last base pair (Fig. 1B).

In a triple-color HSV1(F) strain, VP26 has been tagged at codon 2 with YFP^{VenusA206K}, with this YFP having a mutation that also increases its dissociation constant from 0.11 mM to 74 mM [11,77,78,82]. This strain is indeed infectious in contrast to our HSV1(17^{+})blueLox-YFPVP26$_{\Delta aa\mathbf{5}-7}$, but HSV1(F)-YFP^{VenusA206K}VP26$_{\Delta a1}$ also replicates less well than its parental strain, and induces nuclear aggregates even in Vero cells [11]. An HSV1(F) strain with N-terminal mRFP on VP26 lacking only 4 initial codons but not the authentic non-coding upstream sequences is also infectious; however, in contrast to our HSV1(17^{+})blueLox-mRFPVP26$_{\Delta aa\mathbf{1}-7}$ reported here, this strain also induces nuclear aggregates late in infection, and it is a bit attenuated in Vero cells, too [4]. Furthermore, a PrV-mRFPVP26 strain with authentic upstream sequences and mRFP located between codon 2 and 3 also induces nuclear aggregates and forms smaller plaques [44,83].

Thus, it seems more likely that the reduced protein expression due to 50 upstream bp missing, and not the removal of the 4 N-terminal codons contributes to the almost wild type properties of our HSV1(17^{+})blueLox-mRFPVP26$_{\Delta aa1-7}$. We considered that further compensatory mutations might have allowed efficient capsid assembly and nuclear egress of some XFPVP26 mutants. However, when we monitored several independent lots of cells transfected with BAC DNA, there were no signs of any adaption periods during which CFPVP26$_{\Delta aa5-7}$, mRFPVP26$_{\Delta aa1-7}$ or GFPVP26$_{\Delta aa1-7}$ changed from initial slower growth to faster replication cycles. Furthermore, all experiments were conducted with virions of passage 2 or 3 post transfection, and GFPVP26$_{\Delta aa5-7}$ and YFPVP26$_{\Delta aa5-7}$ did not replicate even after prolonged culture. In summary these studies suggest that VP26 can be successfully tagged with FP domains while maintaining infectivity and efficient nuclear capsid egress when the extent of nuclear aggregate formation is kept low.

Nuclear Aggregates do not Contain Capsids

In contrast to de Oliveira et al. (2008), we could detect the tagged VP26, VP5 (MAb 5C10), pUL17 and pUL25 not only on the rim but also within the nuclear aggregates. The aggregates resemble so-called assemblons that can form with HSV1(F) as early as 6 h but become prominent at 16 h of infection, and that also contain the capsid proteins VP5 and VP19c [84,85]. Ward et al. (1996) therefore suggested that assemblons represent the nuclear site of capsid assembly [84]. Consistent with this hypothesis the nuclear aggregates also contained the scaffolding protein VP22a and the minor capsid proteins pUL17 and pUL25 (c.f. Table 1).

In our analysis, we used four different MAbs raised against VP5: LP12 and H1.4 that detect both, soluble VP5 and capsids, as well as 5C10 and 8F5 that recognize mature hexon epitopes on capsids whose formation requires ATP, proteolytic cleavage of the capsid scaffold and VP26 [5,56,62,86–90]. However, only 5C10 labeled the entire aggregates whereas 8F5, LP12, and H1.4, and also the PAb anti-LC were restricted to their periphery, and after transfection with pHSV1(17^{+})blueLox-GFPVP26$_{\Delta aa\mathbf{5}-7}$ the 8F5 epitope could not be detected at all (c.f. Table 1). Chi & Wilson (2000) suggested that the tag on GFPVP26$_{\Delta aa\mathbf{1}-7}$ may interfere with 8F5 but not 5C10 binding, and we have also reported that 8F5 and 5C10 prefer untagged over HSV1(KOS)-GFPVP26$_{\Delta aa\mathbf{1}-7}$ capsids [5]. However, PAb anti-LC recognizes capsids irrespective of the tag, and LP12 even prefers HSV1(KOS)-GFPVP26$_{\Delta aa\mathbf{1}-7}$ over wild type capsids [5], whereas the nuclear aggregates described here exposed LC and LP12 epitopes only in their periphery. These immunological data are inconsistent with the notion that the nuclear aggregates are conglomerations of authentic progeny capsids. Furthermore, our correlative light and electron microscopy studies showed that many of the nuclear aggregates lack capsids. We therefore conclude that the aggregates are not some sort of capsid assemblons, but may represent an accumulation of dead-end products as also suggested by Lamberti & Weller (1998) and de Bruyn Kops et al. (1998) [69,72]; nevertheless, they may abut areas enriched for capsids.

Therefore, in contrast to what we [8] and others have suggested, a recruitment of viral or host proteins to these nuclear aggregates containing VP5, VP22a, VP26, pUL17 and pUL25 does not indicate that they interact with authentic capsids. Our data rather suggest that these aggregates confiscate so much capsid proteins and possibly other proteins interacting with VP26 that proper capsid assembly and nuclear egress are no longer possible. In our experiments, even pUL36 had been sequestered by the nuclear aggregates in some few cells, although pUL36 usually does not associate with nuclear but only with cytoplasmic capsids [63]. Furthermore, Luxton et al. (2006) [91] reported that deleting UL36 in a PrV strain whose capsids have been tagged with GFPVP26 results in impaired nuclear egress whereas capsids of untagged PrV or HSV1 strains are still exported to the cytoplasm in the absence of pUL36 [63,92–94]. Thus, two mutations with moderate phenotypes, namely a tag on VP26 and deletion of UL36, if combined might potentiate and result in a synthetic phenotype [45,46], in this case impediment of nuclear egress. Such a crosstalk between different mutated proteins might be used to reveal subtle phenotypes which cannot be elucidated otherwise. Moreover, small chemical compounds fostering aggregation of VP26 might be developed into effective antiviral therapy that prevents HSV nuclear capsid egress and thus virion formation. On the other hand, for characterization of intracellular capsid trafficking, virion assembly and cell entry, we will base future tagging or disabling mutations in HSV1 proteins on HSV1(17^{+})-mRFPVP26$_{\Delta aa\mathbf{1}-7}$ that has a low propensity for nuclear aggregation, and therefore seems to contain a less invasive tag on VP26. Furthermore, its subcellular capsid distribution during the course

of an infection resembles more that of untagged capsids when compared to the other tags on VP26.

Acknowledgments

We thank Anja Pohlmann, Anna Buch, Daniela Kieneke, Deepika Devadas, Eva Borst, Fenja Anderson, Randi Diestel and Malte Sandbaumhüter for their comments on the manuscript, and Christof Bohnen and Julia Schipke for support with BAC-mutagenesis (Institute of Virology, Hannover Medical School) as well as Joel Baines (Cornell University, USA) and Prashant Desai (Johns Hopkins University, Baltimore, MD) for helpful discussions. We are grateful to John Subak-Sharpe (MRC Virology Unit, Glasgow, UK) and Prashant Desai for providing HSV1 strains. We thank Susanne Bailer (Fraunhofer Institute for Interfacial Engineering and Biotechnology, Stuttgart, Germany), Jay Brown and Bill Newcomb (University of Virginia, Charlottesville, VA), Edouard Cantin (City of Hope National Medical Center, Duarte, California), Richard J. Courtney (Pennsylvania State University College of Medicine, Hershey, PA), Prashant Desai, Roselyn Eisenberg and Gary Cohen (University of Pennsylvania, Philadelphia, PA), Regine Heilbronn (Charité-UniversitΔtsmedizin, Berlin, Germany), Ari Helenius (Eidgenössische Technische Hochschule Zürich, Switzerland), Helena Browne and Anthony Minson (University of Cambridge, UK), Valerie Preston (MRC Virology Unit, Glasgow, UK), Bernard Roizman (University of Chicago, Chicago, Illinois), and Dan Tenney (Bristol-Myers Squibb, Wallingford, CT) for donating invaluable antibodies. We furthermore acknowledge the support of the Research Core Units for Laser Microscopy and Electron Microscopy at Hannover Medical School.

Author Contributions

Conceived and designed the experiments: CHN KD RB BS. Analyzed the data: CHN KD AB RB BS. Wrote the paper: CHN KD BS.

References

1. Bosse JB, Bauerfeind R, Popilka L, Marcinowski L, Taeglich M, et al. (2012) A Beta-herpesvirus with fluorescent capsids to study transport in living cells. PLoS One 7: e40585.
2. Antinone SE, Zaichick SV, Smith GA (2010) Resolving the assembly state of herpes simplex virus during axon transport by live-cell imaging. J Virol 84: 13019–30.
3. Cheng SB, Ferland P, Webster P, Bearer EL (2011) Herpes Simplex Virus Dances with Amyloid Precursor Protein while Exiting the Cell. PLoS One 6: e17966.
4. de Oliveira AP, Glauser DL, Laimbacher AS, Strasser R, Schraner EM, et al. (2008) Live visualization of herpes simplex virus type 1 compartment dynamics. J Virol 82: 4974–90.
5. Döhner K, Radtke K, Schmidt S, Sodeik B (2006) Eclipse phase of herpes simplex virus type 1 infection: Efficient dynein-mediated capsid transport without the small capsid protein VP26. J Virol 80: 8211–24.
6. Forest T, Barnard S, Baines JD (2005) Active intranuclear movement of herpesvirus capsids. Nat Cell Biol 7: 429–31.
7. Krautwald M, Maresch C, Klupp BG, Fuchs W, Mettenleiter TC (2008) Deletion or green fluorescent protein tagging of the pUL35 capsid component of pseudorabies virus impairs virus replication in cell culture and neuroinvasion in mice. J Gen Virol 89: 1346–51.
8. Nagel CH, Döhner K, Fathollahy M, Strive T, Borst EM, et al. (2008) Nuclear egress and envelopment of herpes simplex virus capsids analyzed with dual-color fluorescence HSV1(17+). J Virol 82: 3109–24.
9. Shanda SK, Wilson DW (2008) UL36p is required for efficient transport of membrane-associated herpes simplex virus type 1 along microtubules. J Virol 82: 7388–94.
10. Smith GA, Gross SP, Enquist LW (2001) Herpesviruses use bidirectional fast-axonal transport to spread in sensory neurons. Proc Natl Acad Sci U S A 98: 3466–70.
11. Sugimoto K, Uema M, Sagara H, Tanaka M, Sata T, et al. (2008) Simultaneous tracking of capsid, tegument, and envelope protein localization in living cells infected with triply fluorescent herpes simplex virus 1. J Virol 82: 5198–211.
12. Wisner TW, Sugimoto K, Howard PW, Kawaguchi Y, Johnson DC (2011) Anterograde transport of herpes simplex virus capsids in neurons by both Separate and Married mechanisms. J Virol 85: 5919–28.
13. Wolfstein A, Nagel CH, Radtke K, Döhner K, Allan VJ, et al. (2006) The inner tegument promotes herpes simplex virus capsid motility along microtubules in vitro. Traffic 7: 227–37.
14. Booy FP, Trus BL, Newcomb WW, Brown JC, Conway JF, et al. (1994) Finding a needle in a haystack: detection of a small protein (the 12-kDa VP26) in a large complex (the 200-MDa capsid of herpes simplex virus). Proc Natl Acad Sci U S A 91: 5652–6.
15. Trus BL, Homa FL, Booy FP, Newcomb WW, Thomsen DR, et al. (1995) Herpes simplex virus capsids assembled in insect cells infected with recombinant baculoviruses: structural authenticity and localization of VP26. J Virol 69: 7362–6.
16. Zhou ZH, He J, Jakana J, Tatman JD, Rixon FJ, et al. (1995) Assembly of VP26 in herpes simplex virus-1 inferred from structures of wild-type and recombinant capsids. Nat Struct Biol 2: 1026–30.
17. Lo P, Yu X, Atanasov I, Chandran B, Zhou ZH (2003) Three-dimensional localization of pORF65 in Kaposi's sarcoma-associated herpesvirus capsid. J Virol 77: 4291–7.
18. Yu X, Shah S, Atanasov I, Lo P, Liu F, et al. (2005) Three-dimensional localization of the smallest capsid protein in the human cytomegalovirus capsid. J Virol 79: 1327–32.
19. Borst EM, Mathys S, Wagner M, Muranyi W, Messerle M (2001) Genetic evidence of an essential role for cytomegalovirus small capsid protein in viral growth. J Virol 75: 1450–8.
20. Desai P, DeLuca NA, Person S (1998) Herpes simplex virus type 1 VP26 is not essential for replication in cell culture but influences production of infectious virus in the nervous system of infected mice. Virology 247: 115–24.
21. Antinone SE, Shubeita GT, Coller KE, Lee JI, Haverlock-Moyns S, et al. (2006) The Herpesvirus capsid surface protein, VP26, and the majority of the tegument proteins are dispensable for capsid transport toward the nucleus. J Virol 80: 5494–8.
22. Henson BW, Perkins EM, Cothran JE, Desai P (2009) Self-assembly of Epstein-Barr virus capsids. J Virol 83: 3877–90.
23. Perkins EM, Anacker D, Davis A, Sankar V, Ambinder RF, et al. (2008) Small capsid protein pORF65 is essential for assembly of Kaposi's sarcoma-associated herpesvirus capsids. J Virol 82: 7201–11.
24. Chen DH, Jakana J, McNab D, Mitchell J, Zhou ZH, et al. (2001) The pattern of tegument-capsid interaction in the herpes simplex virus type 1 virion is not influenced by the small hexon-associated protein VP26. J Virol 75: 11863–7.
25. Chaudhuri V, Sommer M, Rajamani J, Zerboni L, Arvin AM (2008) Functions of Varicella-zoster virus ORF23 capsid protein in viral replication and the pathogenesis of skin infection. J Virol 82: 10231–46.
26. Desai P, Akpa JC, Person S (2003) Residues of VP26 of herpes simplex virus type 1 that are required for its interaction with capsids. J Virol 77: 391–404.
27. McGeoch DJ, Dalrymple MA, Davison AJ, Dolan A, Frame MC, et al. (1988) The complete DNA sequence of the long unique region in the genome of herpes simplex virus type 1. J Gen Virol 69 (Pt 7): 1531–74.
28. Wingfield PT, Stahl SJ, Thomsen DR, Homa FL, Booy FP, et al. (1997) Hexon-only binding of VP26 reflects differences between the hexon and penton conformations of VP5, the major capsid protein of herpes simplex virus. J Virol 71: 8955–61.
29. Baker ML, Jiang W, Wedemeyer WJ, Rixon FJ, Baker D, et al. (2006) Ab initio modeling of the herpesvirus VP26 core domain assessed by CryoEM density. PLoS Comput Biol 2: e146.
30. Baines JD (2011) Herpes simplex virus capsid assembly and DNA packaging: a present and future antiviral drug target. Trends Microbiol 19: 606–13.
31. Homa FL, Brown JC (1997) Capsid assembly and DNA packaging in herpes simplex virus. Rev Med Virol 7: 107–122.
32. Rixon FJ, Addison C, McGregor A, Macnab SJ, Nicholson P, et al. (1996) Multiple interactions control the intracellular localization of the herpes simplex virus type 1 capsid proteins. J Gen Virol 77 (Pt 9): 2251–60.
33. Apcarian A, Cunningham AL, Diefenbach RJ (2010) Identification of binding domains in the herpes simplex virus type 1 small capsid protein pUL35 (VP26). J Gen Virol 91: 2659–63.
34. Bowman BR, Baker ML, Rixon FJ, Chiu W, Quiocho FA (2003) Structure of the herpesvirus major capsid protein. Embo J 22: 757–65.
35. Cardone G, Newcomb WW, Cheng N, Wingfield PT, Trus BL, et al. (2012) The UL36 Tegument Protein of Herpes Simplex Virus 1 Has a Composite Binding Site at the Capsid Vertices. J Virol
36. Zhou ZH, Chen DH, Jakana J, Rixon FJ, Chiu W (1999) Visualization of tegument-capsid interactions and DNA in intact herpes simplex virus type 1 virions. J Virol 73: 3210–8.
37. Lee JH, Vittone V, Diefenbach E, Cunningham AL, Diefenbach RJ (2008) Identification of structural protein-protein interactions of herpes simplex virus type 1. Virology 378: 347–54.
38. Ko DH, Cunningham AL, Diefenbach RJ (2010) The major determinant for addition of tegument protein pUL48 (VP16) to capsids in herpes simplex virus

type 1 is the presence of the major tegument protein pUL36 (VP1/2). J Virol 84: 1397–405.
39. Douglas MW, Diefenbach RJ, Homa FL, Miranda-Saksena M, Rixon FJ, et al. (2004) Herpes simplex virus type 1 capsid protein VP26 interacts with dynein light chains RP3 and Tctex1 and plays a role in retrograde cellular transport. J Biol Chem 279: 28522–30.
40. Wang L, Liu L, Che Y, Wang L, Jiang L, et al. (2010) Egress of HSV-1 capsid requires the interaction of VP26 and a cellular tetraspanin membrane protein. Virol J 7: 156.
41. Radtke K, Kieneke D, Wolfstein A, Michael K, Steffen W, et al. (2010) Plus- and minus-end directed microtubule motors bind simultaneously to herpes simplex virus capsids using different inner tegument structures. PLoS Pathog 6: e1000991.
42. Desai P, Person S (1998) Incorporation of the green fluorescent protein into the herpes simplex virus type 1 capsid. J Virol 72: 7563–8.
43. Snyder A, Wisner TW, Johnson DC (2006) Herpes simplex virus capsids are transported in neuronal axons without an envelope containing the viral glycoproteins. J Virol 80: 11165–77.
44. Bohannon KP, Sollars PJ, Pickard GE, Smith GA (2012) Fusion of a fluorescent protein to the pUL25 minor capsid protein of pseudorabies virus allows live-cell capsid imaging with negligible impact on infection. J Gen Virol 93: 124–9.
45. Nijman SM (2011) Synthetic lethality: general principles, utility and detection using genetic screens in human cells. FEBS Lett 585: 1–6.
46. Tucker CL, Fields S (2003) Lethal combinations. Nat Genet 35: 204–5.
47. Sodeik B, Ebersold MW, Helenius A (1997) Microtubule-mediated transport of incoming herpes simplex virus 1 capsids to the nucleus. J Cell Biol 136: 1007–21.
48. Brown SM, Ritchie DA, Subak-Sharpe JH (1973) Genetic studies with herpes simplex virus type 1. The isolation of temperature-sensitive mutants, their arrangement into complementation groups and recombination analysis leading to a linkage map. J Gen Virol 18: 329–46.
49. Döhner K, Wolfstein A, Prank U, Echeverri C, Dujardin D, et al. (2002) Function of dynein and dynactin in herpes simplex virus capsid transport. Mol Biol Cell 13: 2795–809.
50. Cohen GH, Ponce de Leon M, Diggelmann H, Lawrence WC, Vernon SK, et al. (1980) Structural analysis of the capsid polypeptides of herpes simplex virus types 1 and 2. J Virol 34: 521–31.
51. Koslowski KM, Shaver PR, Wang XY, Tenney DJ, Pederson NE (1997) The pseudorabies virus UL28 protein enters the nucleus after coexpression with the herpes simplex virus UL15 protein. J Virol 71: 9118–23.
52. Ali MA, Forghani B, Cantin EM (1996) Characterization of an essential HSV-1 protein encoded by the UL25 gene reported to be involved in virus penetration and capsid assembly. Virology 216: 278–83.
53. McNabb DS, Courtney RJ (1992) Analysis of the UL36 open reading frame encoding the large tegument protein (ICP1/2) of herpes simplex virus type 1. J Virol 66: 7581–4.
54. Munger J, Chee AV, Roizman B (2001) The U(S)3 protein kinase blocks apoptosis induced by the d120 mutant of herpes simplex virus 1 at a premitochondrial stage. J Virol 75: 5491–7.
55. Ott M, Tascher G, Hassdenteufel S, Zimmermann R, Haas J, et al. (2011) Functional characterization of the essential tail anchor of the herpes simplex virus type 1 nuclear egress protein pUL34. J Gen Virol 92: 2734–2745.
56. Trus BL, Newcomb WW, Booy FP, Brown JC, Steven AC (1992) Distinct monoclonal antibodies separately label the hexons or the pentons of herpes simplex virus capsid. Proc Natl Acad Sci U S A 89: 11508–12.
57. Phelan A, Dunlop J, Patel AH, Stow ND, Clements JB (1997) Nuclear sites of herpes simplex virus type 1 DNA replication and transcription colocalize at early times postinfection and are largely distinct from RNA processing factors. J Virol 71: 1124–32.
58. Newcomb WW, Trus BL, Cheng N, Steven AC, Sheaffer AK, et al. (2000) Isolation of herpes simplex virus procapsids from cells infected with a protease-deficient mutant virus. J Virol 74: 1663–73.
59. Thurlow JK, Rixon FJ, Murphy M, Targett-Adams P, Hughes M, et al. (2005) The herpes simplex virus type 1 DNA packaging protein UL17 is a virion protein that is present in both the capsid and the tegument compartments. J Virol 79: 150–8.
60. Huang AS, Wagner RR (1964) Penetration of Herpes Simplex Virus into Human Epidermoid Cells. Proc Soc Exp Biol Med 116: 863–9.
61. Laemmli UK (1970) Cleavage of structural proteins during the assembly of the head of bacteriophage T4. Nature 227: 680–5.
62. Rode K, Döhner K, Binz A, Glass M, Strive T, et al. (2011) Uncoupling uncoating of herpes simplex virus genomes from their nuclear import and gene expression. J Virol 85: 4271–83.
63. Schipke J, Pohlmann A, Diestel R, Binz A, Rudolph K, et al. (2012) The C Terminus of the Large Tegument Protein pUL36 Contains Multiple Capsid Binding Sites That Function Differently during Assembly and Cell Entry of Herpes Simplex Virus. J Virol 86: 3682–700.
64. Jirmo AC, Nagel CH, Bohnen C, Sodeik B, Behrens GM (2009) Contribution of direct and cross-presentation to CTL immunity against herpes simplex virus 1. J Immunol 182: 283–92.
65. Leelawong M, Lee JI, Smith GA (2012) Nuclear egress of pseudorabies virus capsids is enhanced by a subspecies of the large tegument protein that is lost upon cytoplasmic maturation. J Virol 86: 6303–14.
66. Johnson DC, Baines JD (2011) Herpesviruses remodel host membranes for virus egress. Nat Rev Microbiol 9: 382–94.
67. Mettenleiter TC, Klupp BG, Granzow H (2009) Herpesvirus assembly: an update. Virus Res 143: 222–34.
68. Simpson-Holley M, Colgrove RC, Nalepa G, Harper JW, Knipe DM (2005) Identification and functional evaluation of cellular and viral factors involved in the alteration of nuclear architecture during herpes simplex virus 1 infection. J Virol 79: 12840–51.
69. de Bruyn Kops A, Uprichard SL, Chen M, Knipe DM (1998) Comparison of the intranuclear distributions of herpes simplex virus proteins involved in various viral functions. Virology 252: 162–78.
70. Livingston CM, DeLuca NA, Wilkinson DE, Weller SK (2008) Oligomerization of ICP4 and rearrangement of heat shock proteins may be important for herpes simplex virus type 1 prereplicative site formation. J Virol 82: 6324–36.
71. Ward SA, Weller SK (2011) HSV1 DNA replication. In: Weller, SK editors. Alphaherpesviruses: Molecular Virology. Norfolk, UK: Caister Academic Press. 89–112.
72. Lamberti C, Weller SK (1998) The herpes simplex virus type 1 cleavage/packaging protein, UL32, is involved in efficient localization of capsids to replication compartments. J Virol 72: 2463–73.
73. Reichelt M, Wang L, Sommer M, Perrino J, Nour AM, et al. (2011) Entrapment of viral capsids in nuclear PML cages is an intrinsic antiviral host defense against varicella-zoster virus. PLoS Pathog 7: e1001266.
74. Reichelt M, Joubert L, Perrino J, Koh AL, Phanwar I, et al. (2012) 3D Reconstruction of VZV Infected Cell Nuclei and PML Nuclear Cages by Serial Section Array Scanning Electron Microscopy and Electron Tomography. PLoS Pathog 8: e1002740.
75. Everett RD (2011) The role of ICP0 in counteracting intrinsic cellular resistance to virus infection. In: Weller, SK editors. Alphaherpesviruses: Molecular Virology. Norfolk, UK: Caister Academic Press. 51–72.
76. Espagne A, Erard M, Madiona K, Derrien V, Jonasson G, et al. (2011) Cyan fluorescent protein carries a constitutive mutation that prevents its dimerization. Biochemistry 50: 437–9.
77. Tsien RY (1998) The green fluorescent protein. Annu Rev Biochem 67: 509–44.
78. Zacharias DA, Violin JD, Newton AC, Tsien RY (2002) Partitioning of lipid-modified monomeric GFPs into membrane microdomains of live cells. Science 296: 913–6.
79. Zeng W, Seward HE, Malnasi-Csizmadia A, Wakelin S, Woolley RJ, et al. (2006) Resonance energy transfer between green fluorescent protein variants: complexities revealed with myosin fusion proteins. Biochemistry 45: 10482–91.
80. Campbell RE, Tour O, Palmer AE, Steinbach PA, Baird GS, et al. (2002) A monomeric red fluorescent protein. Proc Natl Acad Sci U S A 99: 7877–82.
81. Kim DB, Zabierowski S, DeLuca NA (2002) The initiator element in a herpes simplex virus type 1 late-gene promoter enhances activation by ICP4, resulting in abundant late-gene expression. J Virol 76: 1548–58.
82. Nagai T, Ibata K, Park ES, Kubota M, Mikoshiba K, et al. (2002) A variant of yellow fluorescent protein with fast and efficient maturation for cell-biological applications. Nat Biotechnol 20: 87–90.
83. Smith GA, Pomeranz L, Gross SP, Enquist LW (2004) Local modulation of plus-end transport targets herpesvirus entry and egress in sensory axons. Proc Natl Acad Sci U S A 101: 16034–9.
84. Ward PL, Ogle WO, Roizman B (1996) Assemblons: nuclear structures defined by aggregation of immature capsids and some tegument proteins of herpes simplex virus 1. J Virol 70: 4623–31.
85. Kobiler O, Brodersen P, Taylor MP, Ludmir EB, Enquist LW (2011) Herpesvirus replication compartments originate with single incoming viral genomes. MBio 2: e00278–11.
86. Chi JH, Wilson DW (2000) ATP-Dependent localization of the herpes simplex virus capsid protein VP26 to sites of procapsid maturation. J Virol 74: 1468–76.
87. Church GA, Wilson DW (1997) Study of herpes simplex virus maturation during a synchronous wave of assembly. J Virol 71: 3603–12.
88. Dasgupta A, Wilson DW (1999) ATP depletion blocks herpes simplex virus DNA packaging and capsid maturation. J Virol 73: 2006–15.
89. Gao M, Matusick-Kumar L, Hurlburt W, DiTusa SF, Newcomb WW, et al. (1994) The protease of herpes simplex virus type 1 is essential for functional capsid formation and viral growth. J Virol 68: 3702–12.
90. Matusick-Kumar L, Hurlburt W, Weinheimer SP, Newcomb WW, Brown JC, et al. (1994) Phenotype of the herpes simplex virus type 1 protease substrate ICP35 mutant virus. J Virol 68: 5384–94.
91. Luxton GW, Lee JI, Haverlock-Moyns S, Schober JM, Smith GA (2006) The pseudorabies virus VP1/2 tegument protein is required for intracellular capsid transport. J Virol 80: 201–9.
92. Desai PJ (2000) A null mutation in the UL36 gene of herpes simplex virus type 1 results in accumulation of unenveloped DNA-filled capsids in the cytoplasm of infected cells. J Virol 74: 11608–18.
93. Fuchs W, Klupp BG, Granzow H, Mettenleiter TC (2004) Essential function of the pseudorabies virus UL36 gene product is independent of its interaction with the UL37 protein. J Virol 78: 11879–89.
94. Roberts AP, Abaitua F, O'Hare P, McNab D, Rixon FJ, et al. (2009) Differing roles of inner tegument proteins pUL36 and pUL37 during entry of herpes simplex virus type 1. J Virol 83: 105–16.